Accepted Manuscript online: 2022-11-11 Article published online: 2022-12-13

Observation of Rare Tri^{6}Di^9 Imine Cages Using Highly Fluorinated Building Blocks

Tom Fleck-Kunde[a]
Emma H. Wolpert[b]
Laura zur Horst[c]
Robert Oestreich[d]
Christoph Janiak[d]
Kim E. Jelfs[b]
Bernd M. Schmidt*[a]

[a] Institut für Organische Chemie und Makromolekulare Chemie, Heinrich-Heine-Universität Düsseldorf, Universitätsstr. 1, 40225 Düsseldorf, Germany
[b] Department of Chemistry, Molecular Sciences Research Hub, Imperial College London, London W12 0BZ, United Kingdom
[c] Kekulé-Institut für Organische Chemie und Biochemie der Universität Bonn, Gerhard-Domagk-Str. 1, 53121 Bonn, Germany
[d] Institut für Anorganische Chemie und Strukturchemie, Heinrich-Heine-Universität Düsseldorf, Universitätsstr. 1, 40225 Düsseldorf, Germany
* bernd.schmidt@hhu.de

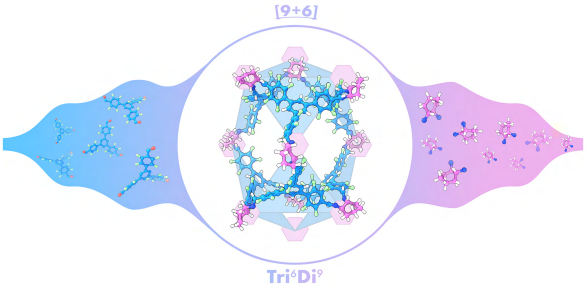

Received: 17. 10. 2022
Accepted after revision: 09.11.2022
DOI: 10.1055/a-1977-1765; Art ID: OM-2022-10-0044-SC

Abstract The first synthesis of organic **Tri^{6}Di^9** cages is presented. Two structurally distinct **Tri^{6}Di^9** cages were synthesised by combining a highly fluorinated aldehyde with two ditopic amines. Although the pure compounds could not be isolated despite many attempts, the information obtained is critical for the future design of large supramolecular structures. Computational and experimental methods indicate that the addition of perfluorinated aromatic linkers in the assembly of porous organic cages opens up new possibilities for influencing the reaction pathway towards rare and unknown structures.

Key words: organic cage compounds, imine cages, dynamic covalent chemistry, fluorine

Introduction

In recent years, the number of reported geometries for porous organic cages (POCs) steadily rose, until it became increasingly more difficult to synthetically access unreported cage topologies.[1] Depending on the functional groups present in the building blocks that constitute the POC, different binding motifs can be exploited in the design of the cage molecules.[2] Focusing on POCs based on dynamic covalent chemistry, imines and boronic ester linkages can be used to construct molecular cages of impressive dimensions.[3] In accordance with the nomenclature proposed by Jelfs et al. in their comprehensive exploration of the topological landscape of POCs, building blocks can be classified as either 'Di' (containing two functional groups), 'Tri' (containing three functional groups) or 'Tet' (containing four functional groups).[4] Combining two components from these three molecule classes leads to a maximum of 20 possible organic cage geometries, most of which have already been reported experimentally. The subclass with the longest history and the most examples is undoubtedly the **Tri^{X}Di^Y** cage family. Ranging from rather small prism-like **Tri^{2}Di^3** imine cages,[5] over **Tri^{4}Di^6** boronic ester cages by Mastalerz and imine cages by Schmidt et al.[6] to the **Tri^{8}Di^{12}** giants from Beuerle and Mastalerz.[7] The wide availability of suitable linkers and the flexibility to vary between tetrahedral and octahedral **Tri^{4}Di^6** cages make this subclass the most versatile of all organic cages.[8] Yet, one geometric member of the **Tri^{X}Di^Y** family remains elusive. To the best of our knowledge, no organic **Tri^{6}Di^9** cage has been reported so far. One possible explanation for this 'missing link' is given by Jelfs et al. during exploration of the energetic landscape for the reaction of 1,3,5-triformylbenzene with (*R*,*R*)-1,2-diaminocyclohexane. The **Tri^{4}Di^6** geometry marks the topology with the lowest relative energy, whereas the relative energy of the **Tri^{6}Di^9** topology is only surpassed by the high relative energy of the **Tri^{2}Di^3** cage. Furthermore, the collapsed **Tri^{6}Di^9** structure is lower in its relative energy compared to the open structure, which, experimentally, could lead to a reduced solubility of the structure, rendering analysis difficult.[4] During their in-

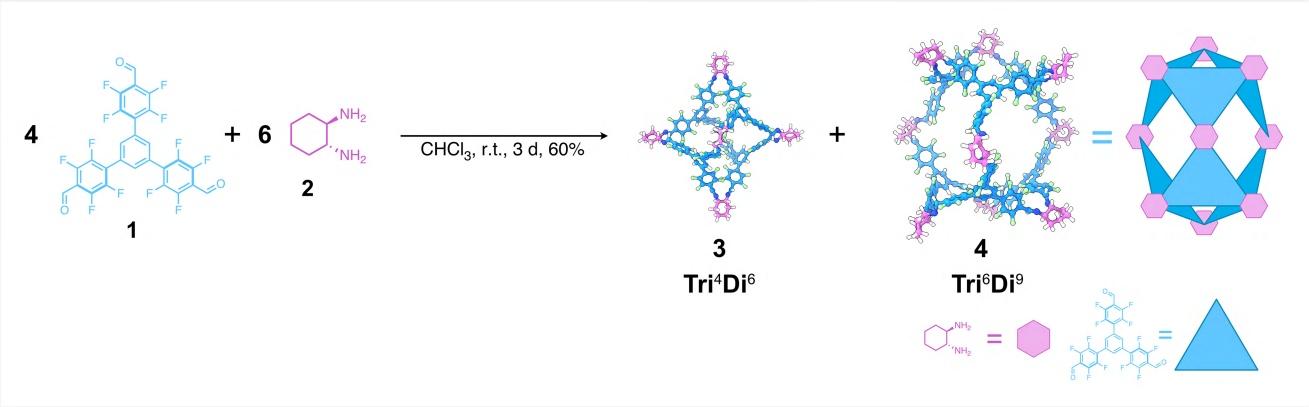

Figure 1 Synthesis of the **Tri**^{4}**Di**^{6} and **Tri**^{6}**Di**^{9} cages from the highly fluorinated aldehyde **1** and the amine **2**. The given yield corresponds to the mixture of products based on aldehyde **1** as the starting material. The open structures of both cages were calculated computationally as described in the computational section at the end of this paper.

vestigation of the templating effects of metals in combination with the bite angles of organic linker molecules, the group of Nitschke reported the formation of a Pd-templated **Tri**^{6}**Di**^{9} structure as a side product along the targeted **Tri**^{4}**Di**^{6} Pd-cage.[9] Both cages proved to be stable in solution and under elevated temperatures for up to 24 hours. Due to the low solubility of both cages, no separation could be conducted successfully, and it was only possible to obtain single crystals of the **Tri**^{4}**Di**^{6} compound. From the ^{1}H NMR spectra, it was deduced that the **Tri**^{6}**Di**^{9}/**Tri**^{4}**Di**^{6} ratio was 1 : 2, and remained unchanged for up to 1 month at 25 °C. This Pd-templated organic cage marks the first report of a quasi-stable **Tri**^{6}**Di**^{9} compound. Herein we report the first non-templated **Tri**^{6}**Di**^{9} compound that can be synthesised from the condensation reaction of a highly fluorinated tritopic aldehyde **1** with the ditopic amine (*R,R*)-1,2-diaminocyclohexane (**2**). Without the stabilizing interactions observed in the Pd-templated structure, we deduce that the flexible, fluorinated linker molecules must play an important role in the compound's formation.

Results and Discussion

When reacting aldehyde **1** with amine **2** in a 1 : 1.5 ratio in chloroform for a period of 3 days at room temperature, two intense signals could be observed in the MALDI MS spectrum (Figures 1 and 2). The stronger signal corresponds very well to ions of the **Tri**^{4}**Di**^{6} cage (**3**) (*m/z* 2894), whereas the signal with a lower intensity can be attributed to the formation of the **Tri**^{6}**Di**^{9} cage ions (**4**) (*m/z* 4340) (see Experimental Section). No traces of the corresponding **Tri**^{2}**Di**^{3} or **Tri**^{8}**Di**^{12} cages could be observed. The formation of two separate species during the synthesis could also be confirmed by NMR analysis. In the ^{1}H NMR, a second set of signals could be observed, which were further analysed in DOSY experiments (Figure 2).

Two distinct species can be observed in the DOSY NMR spectrum, which correspond to solvodynamic radii of r_S = 12.6 Å and r_S = 14.6 Å, respectively. The smaller radius can be attributed to the smaller **Tri**^{4}**Di**^{6} cage, with an approximate spherical radius of 16.1 Å. The larger radius must

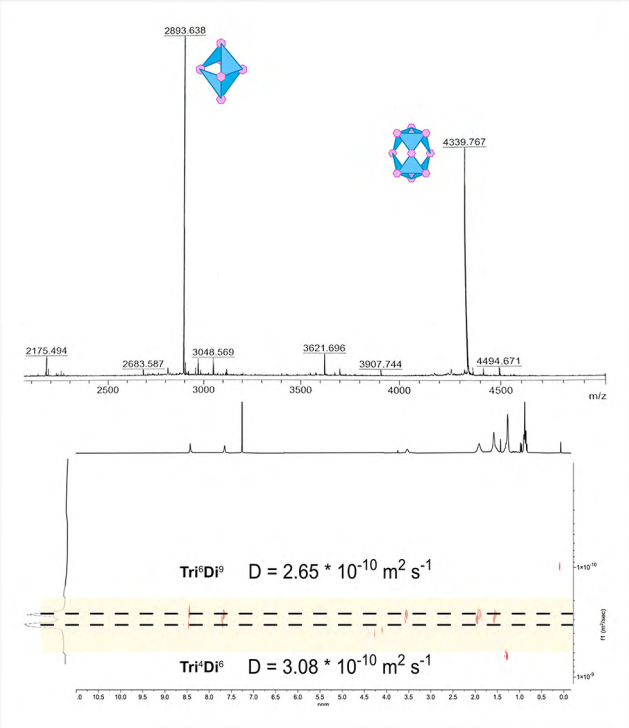

Figure 2 a) MALDI MS spectrum of the isolated precipitate from the reaction mixture; b) ^{1}H DOSY NMR spectrum indicating the presence of two separate species with different diffusion coefficients.

correspond to the **Tri^{6}Di^9** cage, whose spherical radius from the calculated structure is approximately 19.6 Å.

The two cages were formed in an approximate 1 : 1 ratio, as determined by the ^{1}H NMR spectra. Surprisingly, the portion of cage **4** is significantly higher than that observed for the Pd-templated structure (Figure 3). Encouraged by this result, we attempted to optimise the reaction conditions to steer the equilibrium towards the formation of **Tri^{6}Di^9** compound **4** as the sole product. Unfortunately, neither a change in solvent, concentration nor the addition of acid led to an increase of the larger cage compound in the product mixture. The low solubility of **1** in a variety of different organic solvents proved to be a challenge for the reaction optimization, often leading to the formation of an insoluble oligomeric precipitate along with the cage mixture. Increasing the concentration of the starting materials (from 10 to 20 mM) only led to the formation of oligomeric and polymeric structures with no signs of cage formation. Higher dilution surprisingly shifted the equilibrium towards the formation of **Tri^{4}Di^6** cage **3**. This could be explained by the influence of the solvent on the reaction pathway, as the successful cage formation also seems to be solvent-specific. The addition of 2 mol% of trifluoroacetic acid led to the formation of an insoluble precipitate after a short reaction period, hinting at the irreversible formation of insoluble polymeric imine structures.

Although Nitschke et al. were successful in crystallizing one of the cages from a mixture of the two species,[9] all attempts to crystallise the sparingly soluble mixture led either to the formation of an amorphous precipitate (vapor- or layer diffusion) or to a gelation of the chloroform solution containing the cage mixture (slow evaporation).

Separation attempts using recycling gel permeation chromatography (rGPC) were unsuccessful since the sparingly soluble cage mixture decomposed under the basic, high dilution conditions necessary to run the separation experiments. The solubility of the compound mixture in THF was insufficient for separation attempts using different columns. To circumvent this solubility issue, the imine cage mixture was reduced with $NaBH_4$ to yield the corresponding amine cages, which do not undergo reversible bond opening and closing anymore.

Although the reaction of $NaBH_4$ with the imine cage mixture proceeded fast and spontaneously, only a mixture of amine cages with different degrees of reduced imine bonds could be obtained. Elevated temperatures led to the decomposition of both cages, whereas lower temperatures led to a decrease in the number of reduced imine bonds in the product mixture. Although the solubility of the cage mixture was significantly increased by the reduction of the imine bonds, a separation of the mixture via rGPC was unsuccessful due to intense peak broadening.

Since the isolation of **Tri^{6}Di^9** cage **4** could not be accomplished, we investigated the structure of this novel compound computationally. When optimizing the structure of **4**, two outcomes are plausible: i) an open structure in which three aldehydes are connected via three amines in a cyclic arrangement at the top and at the bottom of the macromolecule. These two macrocyclic motifs are then linked at the molecule's equatorial region by three additional ditopic

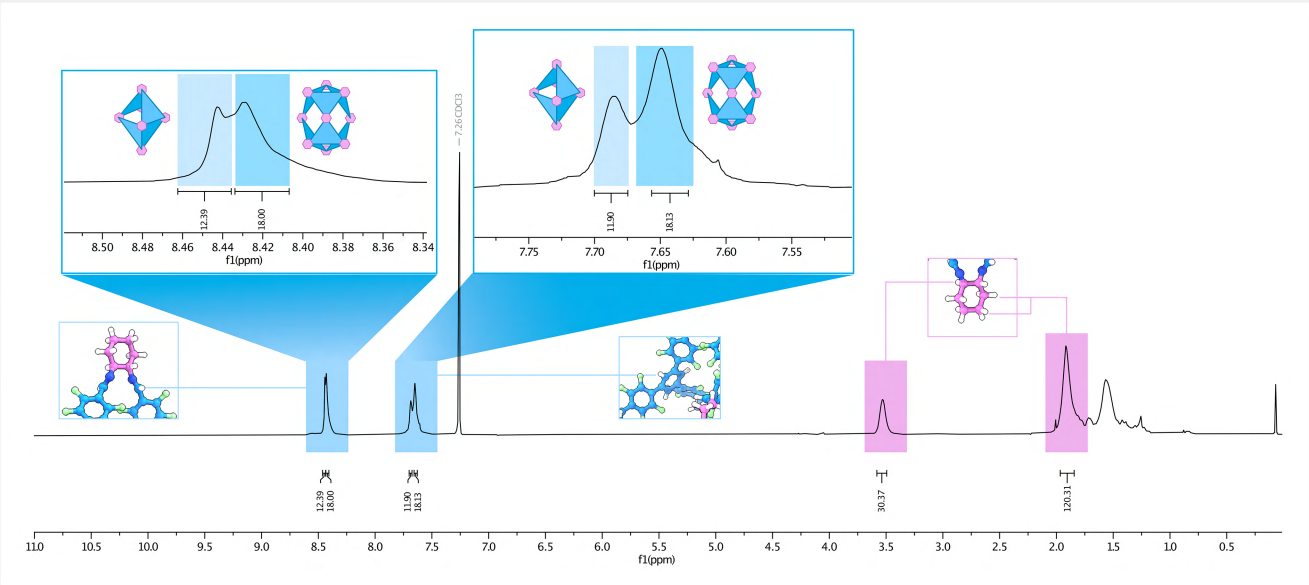

Figure 3 ^{1}H NMR of the imine cage mixture isolated via precipitation from *n*-hexane. Signals that can be assigned to the fluorinated phenylic subunits are highlighted in blue; signals corresponding to the cyclohexyl subunits are highlighted in pink.

amines, resulting in a polyhedral structure that does not correspond to any platonic geometry (Figure 4, left). ii) A collapsed structure in which the interactions between adjacent aromatic motifs are maximised (Figure 4, right).

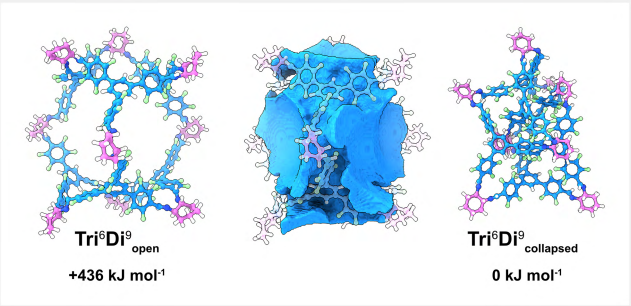

Figure 4 Optimised open structure of **Tri^{6}Di^9** cage **4** and relative energy (left); surface-excluded cavity of the open structure, calculated using MoloVol (center); collapsed structure of **4** and relative energy (right).

Using MoloVol, we estimated the cavity size of $\mathbf{4_{open}}$ to be ≈ 3757 Å^3.[10] If $\mathbf{4_{open}}$ was shape-persistent, the large cavity would make this cage geometry an interesting candidate for use in storage and energy applications. Analogous to the previously discussed investigation of the relative energies inside the **Tri^{X}Di^Y** family, the collapsed structure of **4** is noticeably more stable than the open form (−436 kJ·mol^{-1}). Even if the open form of **4** could be stabilised in solution, the fabrication of a porous material from **4** by solvent removal would prove very challenging. To our surprise, we were able to thermally activate an amorphous sample of the cage mixture and could investigate its gas sorption properties. The cage mixture exhibited a specific surface area of SA_{BET} = 522 m^2·g^{-1} and readily adsorbs 8.97 mmol·g^{-1} of N_2 at 77 K, 3.18 mmol·g^{-1} of H_2 at 77 K, 1.26 mmol·g^{-1} of CO_2 at 273 K, and 0.22 mmol·g^{-1} of CH_4 at 273 K, all at p/p_0 = 1.0 (see Figure S2). The micropore volume (volume of pores smaller than 2 nm) from the N_2 adsorption isotherm at 77 K at a relative pressure p/p_0 of 0.1 is 0.18 cm^3·g^{-1}, and the total pore volume for pores smaller than 20 nm at p/p_0 = 0.95 is 0.30 cm^3·g^{-1}. From the CO_2 non-local density functional theory model at 273 K, a volume of 0.011 cm^3·g^{-1} is calculated for pores with $d \leq 1$ nm (10 Å). This shows that there are only a few ultramicropores (< 0.7 nm) suitable for CO_2 sorption, and the remaining pores are easily accessible for nitrogen. Quenched solid density functional theory calculations on the N_2 isotherm adsorption branch, assuming slit/cylindrical pores in the 'nitrogen at 77 K on carbon' model, yielded a narrow size distribution for pores with a half-pore width around 6.8 Å and mesopores between 17 and 40 Å in half-pore width (see Figure S4 for pore size distribution). This maximum at the half-pore width of 6.8 Å is smaller than the radius of 9.6 Å for a sphere, that would give the cavity volume of 3757 Å^3 of $\mathbf{4_{open}}$. The sorption properties could be attributed to the presence of extrinsic mesoporous cavities due to inefficient packing motifs of either $\mathbf{4_{open}}$ or $\mathbf{4_{collapsed}}$, in addition to the presence of the shape-persistent **3**, although the large cavity volume suggests effects far beyond the individual molecule packing.

To better understand the reason behind the formation of this rare **Tri^{6}Di^9** structure, we decided to investigate the roles of the amine and of the fluorinated aldehyde separately. We therefore combined an isostructural non-fluori-

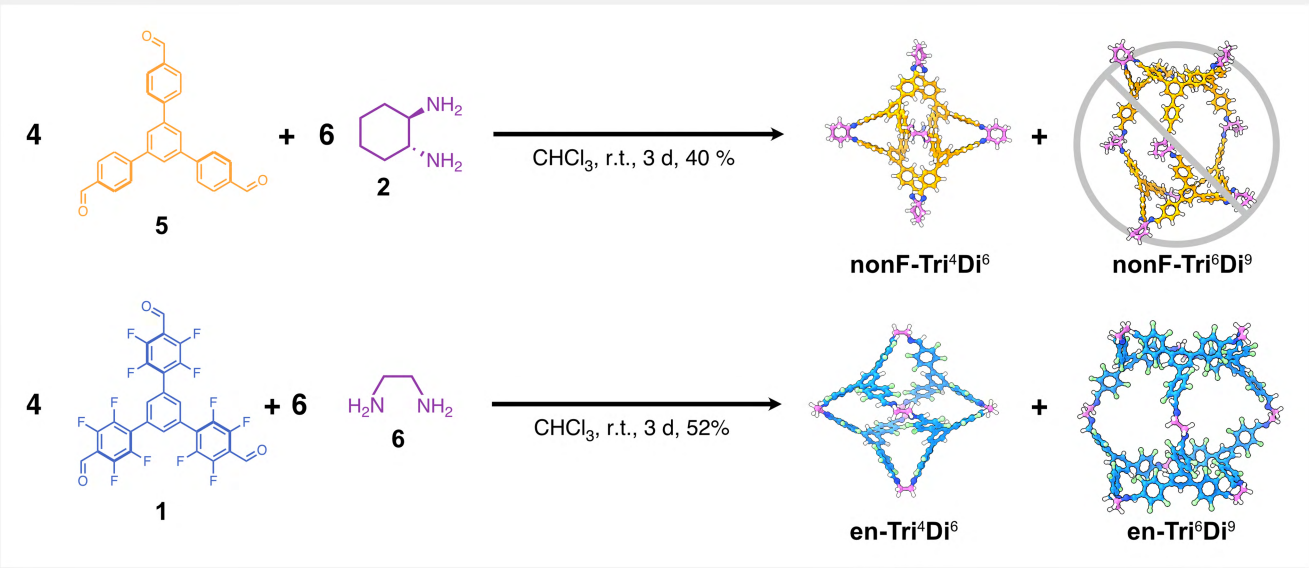

Figure 5 Reaction scheme of non-fluorinated aldehyde **5** with amine **2** (top) and reaction of the fluorinated aldehyde **1** with the flexible diamine **6** (bottom).

nated aldehyde (**5**) with amine **2** and the fluorinated aldehyde **1** with a more flexible amine **6** (Figure 5).

Intriguingly, when the non-fluorinated aldehyde **5** is used, the reaction outcome is much more ill-defined than in the case of aldehyde **1**. During the reaction, significant amounts of polymeric and insoluble oligomeric by-products are formed, and possibly only the **nonF-Tri^{4}Di^6** cage might be identified as part of a mixture with largely oligomeric side products. No trace of the larger **nonF-Tri^{6}Di^9** could be observed in either the ^{1}H NMR or the MALDI MS spectra.

In contrast, when the flexible amine **6** is reacted with the fluorinated aldehyde **1**, the reaction outcome is very similar to the reaction between **1** and **2**. In the ^{1}H NMR, no clear distinction can be made between the signals corresponding to either species as the overlapping of the individual signals is too pronounced (Figure S22). Nevertheless, two distinct signals can be observed in the MALDI MS spectrum, which correspond to the smaller **en-Tri^{4}Di^6** cage and to the larger **en-Tri^{6}Di^9** cage, respectively (Figure S31). From these results, it becomes apparent that the influence of the fluorinated aldehyde must be more pronounced compared to the role of the diamine. Regardless of reacting amine **2** or **6** with the fluorinated aldehyde **1**, the **Tri^{6}Di^9** cage geometry could be observed in both cases, whereas the reaction of the non-fluorinated aldehyde **5** with amine **2** resulted only in the formation of the **Tri^{4}Di^6**-type cages.

Possible explanations could be the electrostatic differences between non-fluorinated and perfluorinated aromatics. Due to the stronger electrostatic repulsions inside **1**, the tetrafluorophenyl units exhibit a larger dihedral angle towards the central aromatic ring. This larger dihedral angle could lead to a clash between neighbouring aldehyde motifs during the imine formation, which leads to the adaptation of a larger bite angle in the corresponding amine. These larger bite angles would result in different angles between two perfluorinated aromatic rings of adjacent aldehyde motifs, which could lead to stabilizing C – F···π_F interactions. These could play a key role in stabilizing the large **Tri^{6}Di^9** geometries. Since the flexible amine **6** is also able to form both the **Tri^{4}Di^6** and the **Tri^{6}Di^9** structures, the contrasting ditopic amine must also exhibit the flexibility to adapt conformationally to this change in geometry.

Conclusions

This work highlights the first synthesis of a purely organic **Tri^{6}Di^9** cage. By using a highly fluorinated aldehyde with two ditopic amines, two structurally different **Tri^{6}Di^9** cages could be synthesised. Although the isolation of the pure compound did not succeed, the information obtained during our study is of significance for the future design of large supramolecular structures. By employing computational and experimental methods, we were able to prove that the introduction of perfluorinated aromatic linkers during the synthesis of POCs opens up new possibilities for influencing the reaction pathway towards rare and unknown structures. By further expanding the libraries of perfluorinated linker molecules, new framework and cage topologies could become accessible that are interesting candidates for use in energy and storage applications alike.

Computational Studies

To determine the thermodynamically most stable form of the structures, we used *stk*[11] to assemble the cages in both the **Tri^{4}Di^6** and **Tri^{6}Di^9** topologies. Using these structures, a high-temperature molecular dynamics run was used to search for the low-energy conformation. The molecular dynamics simulations were run for 5 ns after a 100 ps equilibration with a timestep of 0.5 fs at a temperature of 700 K. Every 50 ps, a structure was sampled and optimised using the OPLS3 force field[12] as implemented in Macromodel.[13] From these simulations, the lowest energy conformation was obtained and compared with the lowest energy open conformation, whose energies were compared.

Experimental Section

The synthesis of the cage mixture containing both **Tri^{4}Di^6** cage **3** and **Tri^{6}Di^9 4** is briefly described below.[14] Detailed experimental procedures and analytical data for building blocks and cages are provided in the Supporting Information. Spectra and NMR assignments are given in the Supporting Information. For details on instrumentation and detailed methods, please refer to the Supporting Information.

Funding Information

T. F.-K. was supported by CHEM CONNECT of HHU Düsseldorf. K. E. J. thanks the Royal Society for a University Research Fellowship and Enhancement Award and the ERC through Agreement No. 758 370 (ERC-StG-PE5-CoMMaD). B. M. S. thanks the North Rhine-Westphalian Academy of Sciences, Humanities and the Arts, and the Deutsche Forschungsgemeinschaft (DFG, German Research Foundation) – SCHM 3101/5 – 1 for funding.

Acknowledgment

We thank Prof. Dr. Guido Clever and Prof. Sigurd Höger for their help with the purification attempts using rGPC.

Supporting Information

Supporting Information for this article is available online at https://doi.org/10.1055/a-1977-1765.

Conflict of Interest

The authors declare no conflict of interest.

References and Notes

(1) (a) Kunde, T.; Pausch, T.; Schmidt, B. M. *Eur. J. Org. Chem.* **2021**, *43*, 5844. (b) Kunde, T.; Nieland, E.; Schröder, H. V; Schalley, C. A.; Schmidt, B. M. *Chem. Commun.* **2020**, *56*, 4761. (c) Beuerle, F.; Gole, B. *Angew. Chem. Int. Ed.* **2018**, *57*, 4850. (d) Greenaway, R. L.; Santolini, V.; Bennison, M. J.; Alston, B. M.; Pugh, C. J.; Little, M. A.; Miklitz, M.; Eden-Rump, E. G. B.; Clowes, R.; Shakil, A.; Cuthbertson, H. J.; Armstrong, H.; Briggs, M. E.; Jelfs, K. E.; Cooper, A. I. *Nat. Commun*. **2018**, *9*, 1. (e) Hasell, T.; Cooper, A. I. *Nat. Rev. Mater.* **2016**, *1*, 16053.

(2) (a) Yang, M.; Qiu, F.; El-Sayed, E. S. M.; Wang, W.; Du, S.; Su, K.; Yuan, D. *Chem. Sci*. **2021**, *12*, 13307. (b) Acharyya, K.; Mukherjee, P. S. *Angew. Chem. Int. Ed*. **2019**, *58*, 8640. (c) Liu, Y.; Zhao, W.; Chen, C. H.; Flood, A. H. *Science* **2019**, *365*, 159. (d) Lee, S.; Yang, A.; Moneypenny, T. P.; Moore, J. S. *J. Am. Chem. Soc.* **2016**, *138*, 2182. (e) Zhang, G.; Mastalerz, M. *Chem. Soc. Rev.* **2014**, *43*, 1934. (f) Stefankiewicz, A. R.; Sambrook, M. R.; Sanders, J. K. M. *Chem. Sci.* **2012**, *3*, 2326.

(3) Zhang, G.; Presly, O.; White, F.; Oppel, I. M.; Mastalerz, M. *Angew. Chem. Int. Ed.* **2014**, *53*, 5126.

(4) Santolini, V.; Miklitz, M.; Berardo, E.; Jelfs, K. E. *Nanoscale* **2017**, *9*, 5280.

(5) (a) Schick, T. H. G.; Rominger, F.; Mastalerz, M. *J. Org. Chem.* **2020**, *85*, 13757. (b) Acharyya, K.; Mukherjee, S.; Mukherjee, P. S. *J. Am. Chem. Soc.* **2013**, *135*, 554. (c) Mastalerz, M.; Schneider, M. W.; Oppel, I. M.; Presly, O. *Angew. Chem. Int. Ed.* **2011**, *50*, 1046. (d) Mateus, P.; Delgado, R.; Brandão, P.; Carvalho, S.; Félix, V. *Org. Biomol. Chem.* **2009**, *7*, 4661. (e) Francesconi, O.; Ienco, A.; Moneti, G.; Nativi, C.; Roelens, S. *Angew. Chem. Int. Ed.* **2006**, *45*, 6693.

(6) (a) Kunde, T.; Pausch, T.; Schmidt, B. M. *Chem. Eur. J.* **2021**, *27*, 8457. (b) Elbert, S. M.; Regenauer, N. I.; Schindler, D.; Zhang, W.-S.; Rominger, F.; Schröder, R. R.; Mastalerz, M. *Chem. Eur. J.* **2018**, *24*, 11438. (c) Schneider, M. W.; Oppel, I. M.; Ott, H.; Lechner, L. G.; Hauswald, H. J. S.; Stoll, R.; Mastalerz, M. *Chem. Eur. J.* **2012**, *18*, 836.

(7) (a) Hähsler, M.; Mastalerz, M. *Chem. Eur. J.* **2021**, *27*, 233. (b) Ivanova, S.; Köster, E.; Holstein, J. J.; Keller, N.; Clever, G. H.; Bein, T.; Beuerle, F. *Angew. Chem. Int. Ed*. **2021**, *60*, 17455. (c) Wagner, P.; Rominger, F.; Zhang, W. S.; Gross, J. H.; Elbert, S. M.; Schröder, R. R.; Mastalerz, M. *Angew. Chem. Int. Ed.* **2021**, *60*, 8896.

(8) (a) Lauer, J. C.; Pang, Z.; Janßen, P.; Rominger, F.; Kirschbaum, T.; Elstner, M.; Mastalerz, M. *ChemistryOpen* **2020**, *9*, 183. (b) Alexandre, P. E.; Zhang, W. S.; Rominger, F.; Elbert, S. M.; Schröder, R. R.; Mastalerz, M. *Angew. Chem. Int. Ed.* **2020**, *59*, 19675. (c) Liu, M.; Zhang, L.; Little, M. A.; Kapil, V.; Ceriotti, M.; Yang, S.; Ding, L.; Holden, D. L.; Balderas-Xicohténcatl, R.; He, D.; Clowes, R.; Chong, S. Y.; Schütz, G.; Chen, L.; Hirscher, M.; Cooper, A. I. *Science* **2019**, *366*, 613. (d) Corcoran Jr, E. W.; Calabro, D. C.; Chong, S. Y.; Chen, L.; Clowes, R.; Hasell, T.; Cooper, A. I. *Angew. Chem. Int. Ed.* **2018**, *57*, 11228. (e) Giri, N.; Del Pópolo, M. G.; Melaugh, G.; Greenaway, R. L.; Rätzke, K.; Koschine, T.; Pison, L.; Gomes, M. F. C.; Cooper, A. I.; James, S. L. *Nature* **2015**, *527*, 216. (f) Ding, H.; Yang, Y.; Li, B.; Pan, F.; Zhu, G.; Zeller, M.; Yuan, D.; Wang, C. *Chem. Commun*. **2015**, *51*, 1976. (g) Mitra, T.; Jelfs, K. E.; Schmidtmann, M.; Ahmed, A.; Chong, S. Y.; Adams, D. J.; Cooper, A. I. *Nat. Chem.* **2013**, *5*, 276.

(9) Lavendomme, R.; Ronson, T. K.; Nitschke, J. R. *J. Am. Chem. Soc.* **2019**, *141*, 12147.

(10) Maglic, J. B.; Lavendomme, R. *J. Appl. Crystallogr.* **2022**, *55*, 1033.

(11) Turcani, L.; Tarzia, A.; Szczypiński, F. T.; Jelfs, K. E. *J. Chem. Phys.* **2021**, *154*, 214102.

(12) Harder, E.; Damm, W.; Maple, J.; Wu, C.; Reboul, M.; Xiang, J. Y.; Wang, L.; Lupyan, D.; Dahlgren, M. K.; Knight, J. L.; Kraus, J. W.; Cerutti, D. S., Krilov; G.; Jorgensen, W. L.; Abel, R.; Friesner, R. A. *J. Chem. Theory Comput.* **2016**, *12*, 281.

(13) Schrödinger Release 2022–3: MacroModel, Schrödinger, LLC, New York, NY, **2021**.

(14) **General procedure:** Synthesis of the cage mixture **Tri^{4}Di^6** and **Tri^{6}Di^9**: Aldehyde **1** (303.20 mg, 0.50 mmol, 1.00 equiv) was dissolved in dry $CHCl_3$ (60 mL) and (*R,R*)-1,2-diaminocyclohexane **2** (79.90 mg, 0.75 mmol, 1.50 equiv) dissolved in 60 mL $CHCl_3$ was added dropwise to the reaction mixture. The resulting solution was stirred at room temperature for 3 days, during which a bright yellow colour developed. Half of the solvent was evaporated under reduced pressure at room temperature, and *n*-hexane was added to the solution, resulting in the precipitation of a bright yellow solid. The solid was isolated by filtration and washed with *n*-hexane to yield **Tri^{4}Di^6** in a mixture with the larger **Tri^{6}Di^9** cage (216.90 mg, 60%) as a yellow solid. **^{1}H NMR** (600 MHz, $CDCl_3$) [δ in ppm] 8.43 (s, 12 H, C**H**N), 7.65 (s, 12 H, Ar-**H**), 3.53 (s, 12 H, C**H**-N), 1.91 (s, 48 H, C**H$_2$**-cyhex). **^{19}F NMR** (282 MHz, $CDCl_3$) [δ in ppm] −142.69 – −143.39 (m, 24F, **F$_{inner}$**), −143.75 (tt, J = 25.4, 13.1 Hz, 24F, **F$_{outer}$**). Due to the very poor solubility, no ^{13}C NMR spectrum could be recorded. **DOSY:** Diffusion coefficient $D = 2.65 \times 10^{-10}$ m^2 s^{-1}. **MALDI MS:** [**Tri^{4}Di^6**+H]$^+$ calculated: 2893.625 *m*/*z*, found: 2893.660 *m*/*z*; [**Tri^{6}Di^9**+H]$^+$ calculated: 4339.940 *m*/*z*, found: 4339.788 *m*/*z*. **FT-IR (ATR):** $\tilde{\nu}$(cm^{-1}) = 2933.73, 2860.43, 2358.94, 2158.35, 1643.35, 1602.85, 1494.83, 1471.69, 1423.47, 1388.75, 1346.31, 1301.95, 1199.72, 1176.58, 1091.71, 1033.85, 991.41, 968.27, 927.76, 891.11, 858.32, 800.46, 777.31, 721.38, 700.16, 677.01, 632.65, 609.51.